From Sun to Earth: Multiscale MHD Simulations of Space Weather

Tamas I. Gombosi[1], Darren L. DeZeeuw[1], Clinton P. T. Groth[2], Kenneth G. Powell[1], C. Robert Clauer[1], and Paul Song[1]

There is an increasing need to develop physics-based, high performance models of the Sun-Earth system — from the solar surface to the Earth's upper atmosphere — which can operate faster than real time and which can provide reliable predictions of the near Earth space environment based upon solar observations and upstream solar wind measurements. Taking advantage of the advent of massively parallel computers, sophisticated solution-adaptive techniques, and recent fundamental advances in basic numerical methods we have developed a high performance, multiscale MHD code capable of resolving many of the critical processes in the Sun-Earth system which range over more than 9 orders of magnitude. We report on the first comprehensive numerical simulation of a "synthetic" space weather event, starting with the generation of a CME and subsequently following this transient solar wind disturbance as it evolves into a magnetic cloud and travels through interplanetary space towards Earth where its interaction with the terrestrial magnetosphere–ionosphere system is also predicted as part of the simulation.

1. INTRODUCTION

"Space Weather" has been used to refer to the conditions on the Sun and in the solar wind, magnetosphere, ionosphere, and thermosphere that can influence the performance and reliability of space-borne and ground based technological systems or can endanger human life or health. A major goal of space weather research is to unify our physical understanding of the Sun-Earth system into a more comprehensive mathematical framework that can predict the deterministic properties of space weather.

Global computational models based on first principles represent a very important component of efforts to understand the intricate processes coupling the Sun to the geospace environment. The hope for such models is that they will eventually fill the gaps left by measurements, extending the spatially and temporarily limited observational database into a self-consistent global understanding of our space environment. Presently, and in the foreseeable future, magnetohydrodynamic (MHD) models are the only models that can span the enormous distances present in the magnetosphere. However, it should not be forgotten that even generalized MHD equations are only a relatively low-order approximation to more complete physics; they provide only a simplified description of natural phenomena in space plasmas.

This paper describes our multiscale MHD model and its application to the Sun-Earth system. The code itself is described in Section 2; the application of the code to simulate a "synthetic" space weather event is described in section 3.

[1]The University of Michigan, Ann Arbor, Michigan, USA

[2]University of Toronto, Toronto, Ontario, Canada

Space Weather
Geophysical Monograph 125

2. SIMULATION CODE

2.1. *Description of BATS-R-US*

The BATS-R-US code solves the governing equations of magnetohydrodynamics. All terms describing deviations

from ideal MHD are included through appropriate source terms. A detailed description of the code can be found in *Powell et al.*, [1999], *Groth et al.*, [1999a] and *De Zeeuw et al.*, [2000]. The code uses a limited reconstruction that ensures second-order accuracy away from discontinuities, while simultaneously providing the stability that ensures nonoscillatory solutions. In addition, the code employs two accurate approximate Riemann solvers: *Roe*'s [1981] scheme [*Powell et al.*, 1999] and *Linde*'s [1998] solver. The resulting scheme solves for the hydrodynamic and electromagnetic effects in a tightly coupled manner, yielding a scheme that works equally well across a range of several orders of magnitude in plasma β.

The basic data structure used in the BATS-R-US approach is that of adaptive blocks [*Stout et al.*, 1997, *Powell et al.*, 1999]. Adaptive blocks partition space into regions, each of which is a regular Cartesian grid of cells, called a block. If the region needs to be refined, then the block is replaced by 8 child subblocks (one for each octant of the parent block), each of which is a Cartesian grid of cells containing the same number of cells as the parent block. If coarsening is needed, then the 8 children are replaced by their parent. The blocks in the grid, at their various levels of refinement, are stored in a tree-like data structure.

2.2. *Non-Ideal MHD Terms*

Ideal MHD is based on the asssumption that the plasma is in local thermodynamic equilibrium. An immediate consequence of this assumption is that no dissipative process can be described by ideal MHD. Even non-ideal MHD equations are only a relatively low order approximation to more complete physics. These equations replace a detailed description of the micro-physics with transport coefficients such as diffusion coefficients, resistivity, and viscosity. In high Reynolds number flows (such as the magnetosphere) viscous effects are usually negligible. However, resistivity and diffusion play important roles in some critical regions of the magnetosphere, and therefore these effects must be included in realistic simulations.

Spatial discretization (an essential element of all numerical solutions) results in numerical dissipation which can mimic the appropriate physical processes. However, numerical resistivity and diffusion in high-resolution modern codes are quite low, and the inclusion of physics-based empirical dissipation coefficients is important. Resistivity is of particular importance, because it controls the rate of magnetic reconnection which is a very important element of the solar wind interaction and global magnetospheric configuration.

Non-ideal MHD processes are included in our MHD model through appropriate terms in the source vector.

2.3. *Simulation Domain*

The computational domain used in the space weather calculation is a heliocentric rectangular box defined by $-32\,R_\odot \le x \le 224\,R_\odot$, $-192\,R_\odot \le y \le 192\,R_\odot$, $-192\,R_\odot \le z \le 192\,R_\odot$. The adapted computational grid for the initial solution of the solar wind (which is a steady-state solution in the corotating frame) consists of 15,768 self-similar $4 \times 4 \times 4$ blocks and 1,009,152 cells with 8 refinement levels and a minimum cell size at the solar surface of 1/16 $R_\odot$. During the time-dependent calculation of the CME, the grid dynamically adapted to the varying solution according to the refinement criteria and the size of the computational mesh varied from under 800,000 cells to in excess of 2,000,000 cells. The length of the entire simulation was 120 hours starting from the initiation of the CME ($t = 0$).

The procedure for prescribing boundary conditions at the solar surface is dependent on local flow conditions. Plasma can freely leave the reservoir, but no "backflow" is allowed. In addition, no deviation is allowed form the intrinsic magnetic field at the interface. At the outer boundaries of the rectangular solution domain, the solar wind flow is essentially super-fast (and hence super-Alfvénic). Simple zero-gradient or constant extrapolation boundary conditions are therefore appropriate and are used to specify the plasma properties at the outer boundary. A detailed description of the boundary conditions can be found in *Groth et al.*, [2000].

The resolution of the initial computational grid at Earth is approximately $10\,R_\odot$, but during the passage of the interplanetary transient this resolution increased by about a factor of four. The embedded magnetosphere is simulated in a moving computational box defined by $-384\,R_E \le x \le 128\,R_E$, $-128\,R_E \le y \le 128\,R_E$, $-128\,R_E \le z \le 128\,R_E$ with 8 levels of refinement, 2004 self-similar blocks of $4 \times 4 \times 4$ cells and 128,256 computational cells. The magnetosphere is "turned on" for a total of 27 hours starting at $t = 70$ h.

The inner boundary of the magnetosphere simulation is a sphere at 3 R_E. This sphere is connected to the height-integrated electrostatic ionosphere.

2.4. *Magnetosphere-Ionosphere Coupling*

The coupling between the magnetosphere and the ionosphere is taken into account through an electrostatic ionosphere model. It is assumed that magnetospheric field-aligned currents can penetrate into the height-integrated electrostatic ionosphere, where the current closure is calculated with the help of Ohm's law using a height-integrated conductivity (conductance) tensor. The model directly relates the normal component of the magnetospheric currents entering the ionosphere through the magnetosphere-ionosphere

interface to the electrostatic potential distribution in the ionosphere. Once the ionospheric electrostatic potential is derived, one can calculate the ionospheric convection velocity, which is used as boundary condition for the magnetosphere simulation at the magnetosphere-ionosphere interface.

2.5. *Applications of BATS-R-US*

BATS-R-US has been extensively applied to global numerical simulations of the Sun-Earth system *Groth et al.*, [1999a], *Gombosi et al.*, [2000c], *Groth et al.* [2000], the coupled terrestrial magnetosphere-ionosphere *Gombosi et al.*, [1998], *Gombosi et al.* [2000a], *Gombosi et al.*, [2000c], *Song et al.*, [1999], *Song et al.*, [2000], and the interaction of the heliosphere with the interstellar medium *Linde et al.*, [1998].

3. A SYNTHETIC SPACE WEATHER EVENT

3.1. *The Inner Heliosphere Near Solar Minimum*

An initial solution representative of the state of the solar wind before the initiation of the CME is required as a starting point for this simulation of a space weather event. A "pre-event" solution has been developed for these purposes using the BATS-R-US simulation code which attempts to reproduce many of the observed global features of solar corona and the inner heliosphere for conditions near solar minimum.

Global computational models based on first principles mathematical descriptions of the physics represent a very important component of efforts to understand the initiation, structure, and evolution of CMEs. Recent examples of the application of MHD models to the study of coronal and solar wind plasma flows include the studies by *Steinolfson* [1994], *Mikić and Linker* [1994], *Suess et al.*, [1996], *Wang et al.*, [1998], *Guo and Wu* [1998], *Lionello et al.*, [1998], *Dryer* [1998], and *Odstrčil and Pizzo* [1999].

In the first part of our simulation we attempted to reproduce the three-dimensional bulk features of the solar wind for solar minimum conditions. We applied the BATS-R-US simulation code to solve the three-dimensionsional ideal MHD equations from the solar surface to beyond Earth's orbit. BATS-R-US has the capability to include the effects of solar rotation, solar gravity, a multipole intrinsic magnetic field (up to octupole), as well as including user-defined volumetric sources of mass, momentum and energy. This feature is very important in the present simulation, since BATS-R-US solves the full MHD energy equation and uses $\gamma = 5/3$ for the ratio of specific heats (since ideal MHD assumes perfect gases).

For the purposes of the present simulation, it is assumed that at the top of transition region, at a radial distance of 1 $R_\odot$, the base of the solar corona is a large rigidly rotating reservoir of hot, stationary plasma with an embedded magnetic multipole field. The plasma temperature (the sum of the ion and electron temperatures) in the reservoir is taken to be $T_\odot = 2.85 \times 10^6$ K and the plasma density is assumed to be $n_\odot = 1.5 \times 10^8$ cm^{-3}.

The intrinsic solar magnetic field at the solar surface is defined in terms of a multipole expansion that includes terms up to the octupole moment. In the present simulation there was no quadrupole moment, while the octupole and dipole were tilted in the (x, z) plane of the corotating coordinate system. The magnetic axis tilt angle was $-15°$ and the solar magnetic field was azimuthally symmetric about the magnetic axis. The surface field strength was 8.4 G at the magnetic poles and 2 G at the solar magnetic equator.

In our simulations we used a volumetric heating function to mimic the combined effects of energy absorption above the transition region, heat conduction (which is not included in ideal MHD) and radiative losses. Presently, the physical understanding of these processes is quite limited, therefore one has considerable freedom in choosing the volumetric heating function. Our approach is to reverse the problem and see whether one can find a heating function which results in reasonable plasma parameters near the Sun and around 1 AU. We adopted a heating function that includes both local energy depositions and losses, thus mimicking the real situation in the lower corona. Specifically, the heating function was assumed to be proportional to $(T_0 - T)$, where T_0 is a prespecified "target" temperature. We have chosen $T_0 = 1.75 T_\odot$ inside the coronal hole and $T_0 = T_\odot$ outside (the coronal hole boundary was at 72.5° latitude). We note that our heating function has a sharp gradient at the edge of the coronal hole, however, the resolution of the computational grid (about 5° near the Sun) limits the sharpness of the transition. Finally, the heating scale-height slowly varies from about 4.5 $R_\odot$ near the equator to about 9 $R_\odot$ at the poles. Overall, the motivation for this choice of heating function was to reproduce many of the observed global plasma properties of the solar wind. A detailed description of the heating function is given in *Groth et al.*, [2000].

Plate 1 shows a 3D representation of the initial solution for the pre-event solar wind near the Sun. The solution is shown in the meridional and equatorial cuts (the (x, z) and (x, y) planes, where the z axis is along the rotation axis, while the magnetic axis is in the (x, z) plane). The color code represents the logarithm of the magnitude of the magnetic field (in units of G) in the two planes. Solid lines are magnetic field lines: magenta denotes the last closed field lines, red is open field lines expanding to the interplanetary medium just above the heliospheric current sheet, and finally, white lines show open magnetic field lines in the (y, z) plane.

The narrow dark blue region in Plate 1 is the beginning of the heliospheric current sheet. It originates around 4 $R_\odot$ where the equatorial portion of the closed magnetic field lines become highly stretched, and extends throughout the entire solution. The current sheet is warped and tilted due to the combined effect of magnetic tilt and rigid solar rotation.

The solution, which is dictated by the complex balance of pressure, magnetic, gravitational, and inertial forces, has regions of open and closed magnetic field lines and leads to the formation of a "helmet" streamer magnetic streamer configuration with associated neutral point and equatorial current sheet. The solution correctly mimics some of the dual state features of the solar wind. It produces fast solar wind ($\sim$ 800 km/s) above $\sim$ 30° heliolatitude, slow ($\sim$ 400 km/s) solar wind near the solar equator, and provides reasonable values for the solar wind temperature and density and interplanetary magnetic field at 1 AU.

Overall, our initial condition represents a very reasonable description of three-dimensional inner heliosphere for solar minimum conditions. We used physically reasonable input parameters near the Sun and were able to obtain a solution out to 1 AU which is in good overall agreement with average observed solar wind conditions.

3.2. Simulation of a CME

Coronal mass ejections (CMEs) are highly transient solar events involving the expulsion of mass and magnetic field from the solar surface. On the order of 10^{12} kg of plasma may be expelled from the solar surface during a typical event. These dynamic events originate in closed magnetic field regions of the corona. They produce large-scale reconfiguration of the coronal magnetic field and generate large solar wind disturbances that, as mentioned above, appear to be the primary cause of major geomagnetic storms at Earth.

The physical mechanisms involved in the initiation of CMEs are not well understood. After release, CMEs accelerate and become part of the outward flow of the solar wind. They are either accelerated by the solar wind so as to come into equilibrium with the ambient wind or act as drivers moving faster than the background solar wind. Close to the Sun, the typical dimension of a CME is less than a solar radius. As the CMEs propagate outward from the corona, they expand dramatically and may extend over tenths of an AU by the time Earth's orbit is reached at 1 AU. Moreover, many, if not all, CMEs are associated with magnetic clouds and the plasma properties within these clouds can differ substantially from those of the ambient solar wind.

Global computational models based on first principles mathematical descriptions of the physics represent a very important component of efforts to understand the initiation, structure, and evolution of CMEs. Here we show our numerical results for a CME driven by local plasma density enhancement. This initial condition represents a simplified model of the situation just before eruption, when significant amount of mass is elevated into the lower corona. Later, we will apply more sophisticated initial conditions. At this time we just wanted to initiate a mass ejection and see how it moves through interplanetary space. In this calculation, the background solar wind solution described above was used as an initial solution and then a localized isothermal density enhancement was introduced at the solar surface just above the equatorial plane (as a consequence of the isothermal assumption the plasma pressure was also increased by the same factor as the density). This localized isothermal density enhancement initiated the CME. In this enhancement the density and pressure are locally increased by a factor of 135 in a small region just above the solar equator for a duration of about 12 hours.

Plate 2 shows a three-dimensional representation of the magnetic field configuration 9 hours after the initiation of the CME. The color code represents $\log(B)$, white lines are open magnetic field lines, magenta lines represent magnetic field lines with both ends connected to the Sun. At this time the density enhancement is in the declining phase, but it is still more than 100 times higher than the background density. The density enhancement first leads to the "filling" of the closed magnetic field lines with additional plasma and subsequent expansion of the closed field line region. One can see that the closed field lines became greatly stretched by the outward moving plasma. This is due to the fact that the plasma β (the ratio of the kinetic and magnetic pressures) is quite large and the magnetic field is "carried" by the outward moving plasma. We also note the decrease of magnetic field strength behind the leading edge of the outward moving disturbance.

A very interesting aspect of simulation results is the anisotropic expansion of the CME. The CME is fairly concentrated near the disrupted heliospheric current sheets, while it is broadly spread in the equatorial plane.

3.3. Interaction with the Magnetosphere

The magnetosphere is a complex nonlinear system. The direction of the interplanetary magnetic field (IMF) fundamentally controls the large-scale topology of the magnetospheric configuration. The magnetospheric topology in turn controls the entry of mass, momentum, energy, and magnetic flux into the magnetosphere. The entry of these physical quantities from the solar wind into the magnetosphere produces various transition layers, the extended geomagnetic tail and the plasma sheet, current systems and auroral phenomena.

Three-dimensional global MHD simulations have been used for a long time to simulate the global magnetospheric

configuration and to investigate the response of the magnetosphere-ionosphere system to changing solar wind conditions. The first global-scale 3D MHD simulations of the solar wind-magnetosphere system were published in the early 1980s. Since then, global 3D MHD simulations have been used to study a range of processes [*Ogino and Walker*1984, *Lyon et al.*, 1986, *Ogino* 1986, *Ogino et al.*, 1986, *Fedder and Lyon* 1987, *Watanabe and Sato* 1990, *Usadi et al.*, 1993, *Walker et al.*, 1993, *Fedder et al*, 1995a,b, *Berchem et al.*, 1995, *Rader et al.*, 1995, *Tanaka* 1995, *Janhunen and Koskinen* 1997, *Raeder et al.*, 1997, *Winglee et al.*, 1997, *Gombosi et al.*, 1998, 2000a, *White et al.*, 1998].

Here, for the first time, we simulate the dynamic response of the global magnetospheric configuration to changing solar wind conditions self-consistently simulated all they way from the Sun to 1 AU. The solar wind changes at the location of the Earth due to the rotation of the tilted solar magnetic field and due to the passage of the coronal ejection described in the previous section.

In the simulation Earth is assumed to move on a perfectly circular orbit about the Sun with an orbital radius of 215.5 R_s and an orbital period of 365.25 days. The orbital plane is assumed to be inclined at an angle of 7.25° to the solar equator with a node line aligned with the x-axis and the maximum and minimum excursions of the planet in z-direction occurring in the $y = 0$ plane. Earth's initial position at $t = 0$ in the numerical simulation is heliolatitude 7.24° and longitude 11.9° (the CME takes place at 0° longitude and 11.5° latitude).

At this position Earth is located near the heliospheric current sheet when the CME is initiated. At Earth's location the first signatures of the CME can be seen in the magnetic field components at around 55 hours after initiation. The driving mass (the piston) arrives around 72 hours after the beginning of the event. The B_y component of the magnetic field remains pretty steady during the entire event, its value only changes by ~ 0.5 nT. The B_x and B_z components, however, exhibit a significant rotation around the y axis. This, in effect, is the signature of the passage of a CME-related flux rope. During the event the magnitude of the IMF increases from about 2 nT to approximately 4 nT. A more detailed description of the solar wind parameters at 1 AU is given in *Groth et al.*, [2000].

The plasma temperature ($T_e + T_p$) in the background solar wind is about 2×10^5K. During the CME (beginning at around 55 hours) the plasma temperature significantly decreases dipping below 1.5×10^5K. The solar wind velocity remains nearly radial during the entire event with the speed gradually decreasing from about 550 km/s to about 450 km/s. The undisturbed solar wind density is fairly high before the CME event ($\sim$ 38 cm^{-3}), but it decreases to a more typical value of ~ 18 cm^{-3} just at the arrival of the piston. At the peak of the event the density increases to about 45 cm^{-3}. The solar wind dynamic pressure increases from its pre-CME value of 2.25 nP (at 72 hours) to 4.6 nP at the peak of the event.

Plate 3 shows the change of the global magnetospheric configuration during the passage of the CME event. The Plate shows two 3D snapshots at $t = 70.5$h and 94.5h. The color code represents the electric current density in the plane of the terrestrial equator, solid lines show last closed magnetic field lines. One can see the magnetopause current (or Chapman-Ferraro current) near the subsolar magnetopause and the tail current on the nightside.

The global magnetospheric configuration is primarily controlled by the B_z component of the interplanetary magnetic field. For $B_z < 0$ the magnetosphere exhibits an open configuration with significant dayside reconnection and open magnetic field lines connected to large regions near the magnetic poles. For strong northward IMF conditions ($B_z >$ 5 nT) the magnetosphere becomes practically closed with magnetic reconnection limited to small regions near the cusps. For "intermediate" values of B_z (between about 0 and 5 nT) the global magnetospheric configuration is "partially closed" (or "partially open"). This configuration is characterized by significant dayside reconnection and large open cusps, by a narrow near-Earth reconnection line around the center of the magnetotail (the length of this reconnection line decreases with increasing B_z), and by long, stretched magnetospheric wings connected to the dawn and dusk sides of the ionosphere. These magnetic wings are formed by highly stretched closed magnetic field lines. They represent the transition from magnetopause reconnection to tail reconnection. In Plate 3 the last closed filed lines at the magnetosphere are shown by green, while the last closed field lines in the tail are shown by red.

During the simulated CME event B_z varies between about 0 nT and 3 nT, therefore the global magnetospheric configuration never switches to pure "South" or "North" configuration. However, the magnetosphere significantly changes during the event. As the solar wind dynamic pressure increases the dayside magnetopause moves inward and the current densities significantly increase. In addition, the magnetosphere becomes narrower and the length of the magnetic wings increases from about 60 R_E to 90 R_E. Overall, the energy and magnetic flux stored in the magnetosphere increased substantially.

A very interesting feature seen in Plate 3 is the clockwise "twist" of the magnetosphere perpendicular to the solar wind direction. This twist, which is particularly visible in the wings, is due to the presence of a non-zero B_y component.

Plate 4 shows the change of ionospheric potential and convection pattern during the CME event. The color code repre-

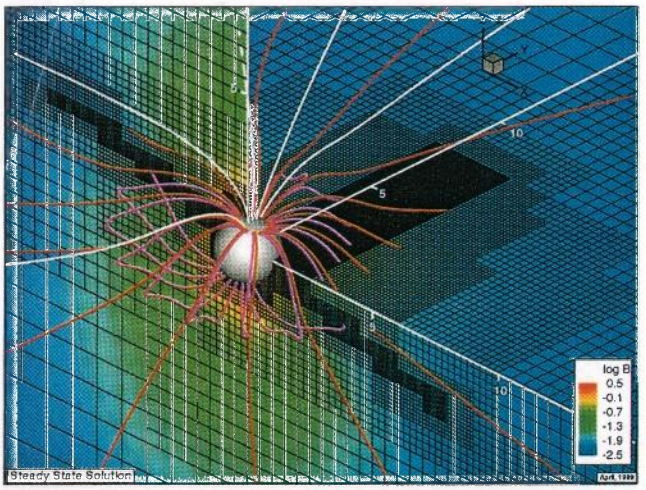

Plate 1. 3D representation of the near solar region before the initiation of the CME. The color code represents $\log(B)$ in the (x, z) and (x, y) planes. Solid lines are magnetic field lines: magenta denotes the last closed field lines, red is open field lines expanding to the interplanetary medium just above the heliospheric current sheet, and finally, white lines show open magnetic field lines in the (y, z) plane.

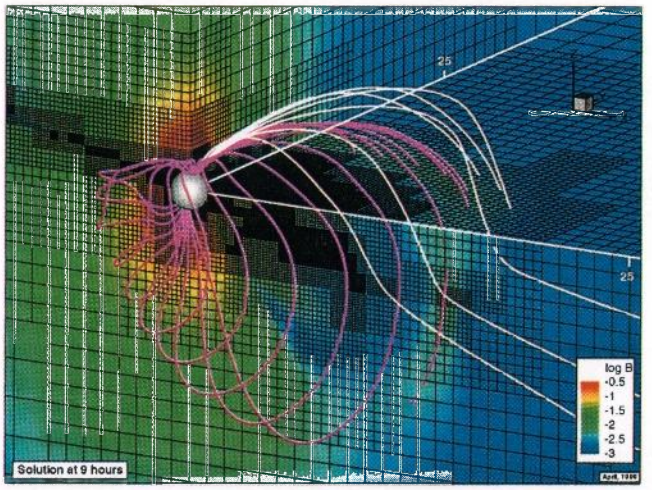

Plate 2. 3D representation magnetic field lines 9 hours after the initiation of a CME. Color code represents $\log(B)$, white lines are open magnetic field lines, magenta lines represent magnetic field lines with both ends connected to the Sun.

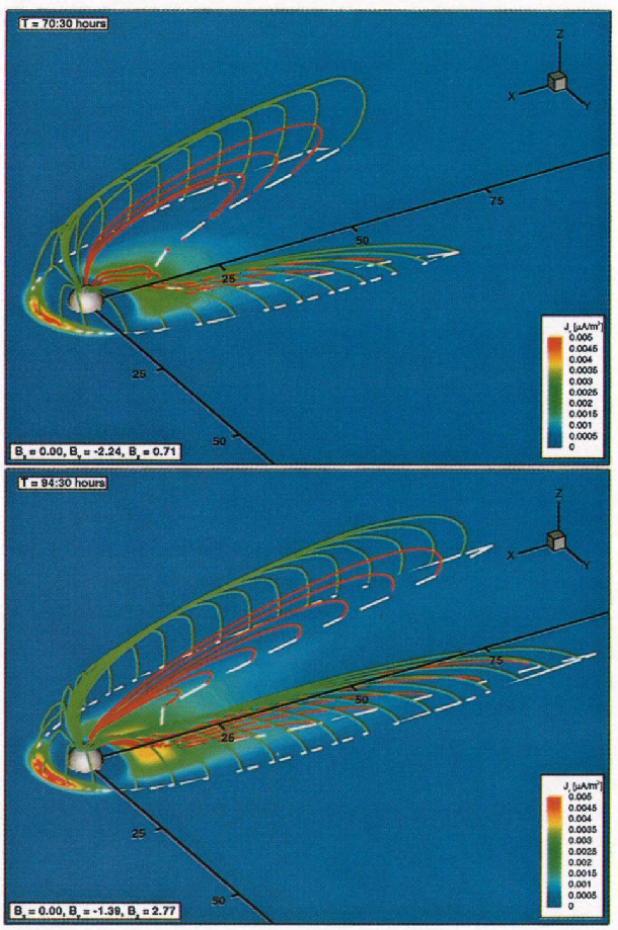

Plate 3. The response of the magnetosphere to the CME.

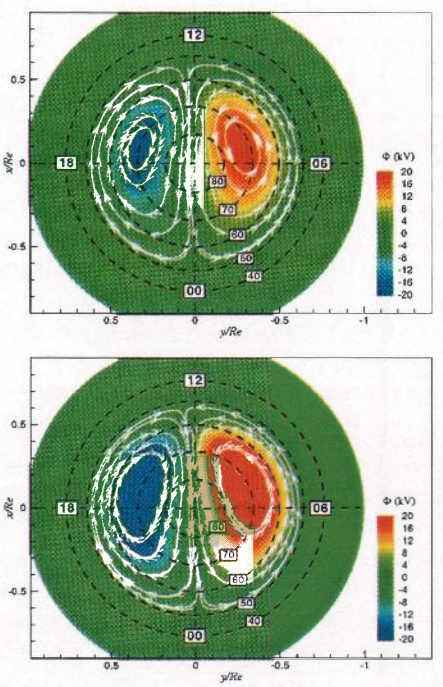

Plate 4. Polar plot of the ionospheric convection (white lines) and potential distribution (color code) in the northern polar ionopshere at $t = 70.5$ h (left panel) and $t = 97.3$ h (right panel).

sents the calculated electric potential in the height-integrated ionosphere, white lines show ionospheric convection patterns. One can see the two-cell pattern of ionospheric convection typical for southward-type IMF conditions. The convection pattern is also "twisted" due to the presence of a nonzero IMF B_y component. The most important change in the ionosphere is the doubling of the cross-cap potential drop from 30 kV at 70.5h to 60 kV some 27 hours later.

Overall, the terrestrial consequences of the simulated space weather event were not "dramatic" due to our choice of initial conditions to drive it. During the event the B_z component of the interplanetary magnetic field never exceeded $+1$ nT, therefore the geoeffectiveness of the CME was quite small. However, the capabilities demonstrated by doing the calculation are themselves dramatic, and nothing precludes us from using the code to simulate more geoeffective events, and ultimately even for forecasting real storms in space. This will be the focus of our upcoming investigations.

Acknowledgments. This work was supported by the NSF KDI grant NSF ATM-9980078, by NSF CISE grant ACI-9876943 and by NASA AISRP grant NAG5-9406.

REFERENCES

Berchem, J., J. Raeder, and M. Ashour-Abdalla, Reconnection at the magnetospheric boundary: Results from global magnetohydrodynamic simulations, in *Physics of the Magnetopause*, edited by P. Song, B. Sonnerup, and M. Thomsen, p. 205, AGU, Washington, D.C., 1995.

De Zeeuw, D. L., T. I. Gombosi, C. P. T. Groth, K. G. Powell, and Q. F. Stout, An adaptive MHD method for global space weather simulations, *IEEE Trans. Plasma Sci.*, in press, 2000.

Dryer, M., Multidimensional, magnetohydrodynamic simulation of solar-generated disturbances: Space weather forecasting of geomagnetic storms, *AIAA Journal, 3*, 365–370, 1998.

Fedder, J. A., and J. G. Lyon, The solar wind-magnetosphere-ionosphere current-voltage, *Geophys. Res. Lett., 14*, 880–883, 1987.

Fedder, J. A., J. G. Lyon, S. P. Slinker, and C. M. Mobarry, Topological structure of the magnetotail as a function of interplanetary magnetic field direction, *J. Geophys. Res., 100*, 3613–3621, 1995a.

Fedder, J. A., S. P. Slinker, J. G. Lyon, and R. D. Elphinstone, Global numerical simulation of the growth phase and the expansion onset for a substorm observed by Viking, *J. Geophys. Res., 100*, 19,083–19,093, 1995b.

Gombosi, T. I., D. L. De Zeeuw, C. P. T. Groth, K. G. Powell, and P. Song, The length of the magnetotail for northward IMF: Results of 3D MHD simulations, in *Physics of Space Plasmas*, edited by T. Chang, and J. R. Jasperse, vol. 15, pp. 121–128, MIT Press, Cambridge, Mass., 1998.

Gombosi, T. I., D. L. De Zeeuw, C. P. T. Groth, and K. G. Powell, Magnetospheric configuration for Parker-spiral IMF conditions: Results of a 3D AMR MHD simulation, *Adv. Space Res., 26*(1), 139–149, 2000a.

Gombosi, T. I., D. L. De Zeeuw, C. P. T. Groth, K. G. Powell, and Q. F. Stout, Multiscale MHD simulation of a coronal mass ejection and its interaction with the magnetosphere-ionosphere system, *J. Atmos. Solar-Terr. Phys., 62*, 1515–1525, 2000b.

Gombosi, T. I., K. G. Powell, and B. van Leer, Comment on "Modeling the magnetosphere for northward interplanetary magnetic field: Effects of electrical resistivity" by Joachim Raeder, *J. Geophys. Res., 105*, 13,141–13,147, 2000c.

Groth, C. P. T., D. L. De Zeeuw, T. I. Gombosi, and K. G. Powell, A parallel adaptive 3D MHD scheme for modeling coronal and solar wind plasma flows, *Space Sci. Rev., 87*, 193–198, 1999a.

Groth, C. P. T., D. L. De Zeeuw, K. G. Powell, T. I. Gombosi, and Q. F. Stout, A parallel solution-adaptive scheme for ideal magnetohydrodynamics, in *Proc. 14th AIAA Computational Fluid Dynamics Conference*, Norfolk, Virginia, AIAA Paper No. 99-3273, 1999b.

Groth, C. P. T., D. L. De Zeeuw, T. I. Gombosi, and K. G. Powell, Global 3D MHD simulation of a space weather event: CME formation, interplanetary propagation, and interaction with the magnetosphere, *J. Geophys. Res., 105*(A11), 25,053 – 25,078, 2000.

Guo, W. P., and S. T. Wu, A magnetohydrodynamic description of coronal helmet streamers containing a cavity, *Astrophys. J., 494*, 419–429, 1998.

Janhunen, P., and H. E. J. Koskinen, The closure of Region-1 field-aligned current in MHD simulation, *Geophys. Res. Lett., 24*(11), 1419–1422, 1997.

Linde, T. J., A three-dimensional adaptive multifluid MHD model of the heliosphere, Ph.D. thesis, Univ. of Mich., Ann Arbor, 1998.

Linde, T. J., T. I. Gombosi, P. L. Roe, K. G. Powell, and D. L. De Zeeuw, The heliosphere in the magnetized local interstellar medium: Results of a 3D MHD simulation, *J. Geophys. Res., 103*(A2), 1889–1904, 1998.

Lionello, R., Z. Mikić, and D. D. Schnack, Magnetohydrodynamics of solar coronal plasmas in cylindrical geometry, *J. Comput. Phys., 140*, 172–201, 1998.

Lyon, J. G., J. Fedder, and J. Huba, The effect of different resistivity models on magnetotail dynamics, *J. Geophys. Res., 91*, 8057–8064, 1986.

Mikić, Z., and J. A. Linker, Disruption of coronal magnetic field arcades, *Astrophys. J., 430*, 898–912, 1994.

Odstrčil, D., and V. J. Pizzo, Distortion of the interplanetary magnetic field by three-dimensional propagation of coronal mass ejections in a structured solar wind, *J. Geophys. Res., 104*, 28,225–28,239, 1999.

Ogino, T., A three-dimensional MHD simulation of the interaction of the solar wind with the Earth's magnetosphere: The generation of field-aligned currents, *J. Geophys. Res., 91*, 6791–6806, 1986.

Ogino, T., and R. J. Walker, A magnetohydrodynamic simulation of the bifurcation of tail lobes during intervals with a northward interplanetary magnetic field, *Geophys. Res. Lett., 11*, 1018–1021, 1984.

Ogino, T., R. Walker, M. Ashour-Abdalla, and J. Dawson, An MHD simulation of the effects of the interplanetary magnetic field B_y component on the interaction of the solar wind with the Earth's magnetosphere during southward interplanetary magnetic field, *J. Geophys. Res., 91*, 10029, 1986.

Powell, K. G., An approximate Riemann solver for magnetohydrodynamics (that works in more than one dimension), Tech. Rep. 94-24, Inst. for Comput. Appl. in Sci. and Eng., NASA Langley Space Flight Center, Hampton, Va., 1994.

Powell, K. G., P. L. Roe, T. J. Linde, T. I. Gombosi, and D. L. D.

Zeeuw, A solution-adaptive upwind scheme for ideal magnetohydrodynamics, *J. Comput. Phys.*, *154*(2), 284–309, 1999.

Raeder, J., R. J. Walker, and M. Ashour-Abdalla, The structure of the distant geomagnetic tail during long periods of northward IMF, *Geophys. Res. Lett.*, *22*, 349–352, 1995.

Raeder, J., J. Berchem, M. Ashour-Abdalla, L. A. Frank, W. R. Paterson, K. L. Ackerson, S. Kokubun, T. Yamamoto, and J. A. Slavin, Boundary layer formation in the magnetotail: Geotail observations and comparisons with a global MHD simulation, *Geophys. Res. Lett.*, *24*, 951–954, 1997.

Roe, P. L., Approximate Riemann solvers, parameter vectors, and difference schemes, *J. Comput. Phys.*, *43*, 357–372, 1981.

Song, P., D. L. De Zeeuw, T. I. Gombosi, C. P. T. Groth, and K. G. Powell, A numerical study of solar wind–magnetosphere interaction for northward IMF, *J. Geophys. Res.*, *104*(A12), 28,361–28,378, 1999.

Song, P., T. Gombosi, D. De Zeeuw, K. Powell, and C. P. T. Groth, A model of solar wind - magnetosphere - ionosphere coupling for due northward IMF, *Planet. Space Sci.*, *48*, 29–39, 2000.

Steinolfson, R. S., Modeling coronal streamers and their eruption, *Space Sci. Rev.*, *70*, 289–294, 1994.

Stout, Q. F., D. L. De Zeeuw, T. I. Gombosi, C. P. T. Groth, H. G. Marshall, and K. G. Powell, Adaptive blocks: A high-performance data structure, in *Proc. Supercomputing'97*, 1997.

Suess, S. T., A.-H. Wang, and S. T. Wu, Volumetric heating in coronal streamers, *J. Geophys. Res.*, *101*(A9), 19,957–19,966, 1996.

Tanaka, T., Generation mechanisms for magnetosphere-ionosphere current systems deduced from a three-dimensional MHD simulation of the solar wind-magnetosphere-ionosphere coupling process, *J. Geophys. Res.*, *100*(A7), 12,057–12,074, 1995.

Usadi, A., A. Kageyama, K. Watanabe, and T. Sato, A global simulation of the magnetosphere with a long tail: Southward and northward interplanetary magnetic field, *J. Geophys. Res.*, *98*, 7503–7517, 1993.

Walker, R. J., T. Ogino, J. Raeder, and M. Ashour-Abdalla, A global magnetohydrodynamic simulation of the magnetosphere when the interpalnetary magnetic field if southward: The onset of magnetotail reconnection, *J. Geophys. Res.*, *98*, 17235, 1993.

Wang, A.-H., S. T. Wu, S. T. Suess, and G. Poletto, Global model of the corona with heat and momentum addition, *J. Geophys. Res.*, *103*, 1913–1922, 1998.

Watanabe, K., and T. Sato, Global simulation of the solar wind-magnetosphere interaction: The importance of its numerical validity, *J. Geophys. Res.*, *95*, 75–88, 1990.

White, W. W., G. L. Siscoe, G. M. Erickson, Z. Kaymaz, N. C. Maynard, K. D. Siebert, B. U. Ö. Sonnerup, and D. R. Weimer, The magnetospheric sash and the cross-tail S, *Geophys. Res. Lett.*, *25*(10), 1605–1608, 1998.

Winglee, R. M., V. O. Papitashvili, and D. R. Weimer, Comparison of the high-latitude ionospheric electrodynamics inferred from global simulations and semiempirical models for the January 1992 GEM campaign, *J. Geophys. Res.*, *102*, 26,961–26,977, 1997.

T. I. Gombosi, D. L. DeZeeuw, C. R. Clauer, and P. Song, Department of Atmospheric and Oceanic Sciences, The University of Michigan, Ann Arbor, MI 48109. (e-mail: tamas@umich.edu, darrens@umich.edu, rclauer@umich.edu, psong@umich.edu)

K. G. Powell, Department of Aerospace Engineering, The University of Michigan, Ann Arbor, MI 48109 (e-mail: powell@umich.edu)

C. P. T. Groth, University of Toronto Institute for Aerospace Studies, 4925 Dufferin St., Toronto, Ontario, Canada, M3H 5T6 (e-mail: groth@utias.utoronto.ca)